

## Chapter 2

# Biochemical Synthesis of Metal Nanoparticles

As already mentioned above, biochemical synthesis is based on the reduction of metal ions in reverse micelles. We realize that the term «biochemical synthesis» is not quite correct as it gives rise to an analogy with the processes of biosynthesis that proceed in living cells and represent one of the subjects studied in biochemistry, while we actually mean the chemical reaction of the reduction of metal ions to atoms by biological molecules, which triggers the process of aggregation of atoms and ions, i.e., the nanoparticle synthesis proper. Similar problem arises at the formal consideration of names of the methods using biological reducing agents («bioreduction», «green synthesis», «biogenic synthesis», also «biochemical synthesis»), described in the previous chapter. In our case, from the different names discussed on the initial stage of the development of this method, it was only the «biochemical synthesis in reverse micelles» that was finely established, since it reflects, on the one hand, the fundamental difference from chemical methods using non-biological reducing agents in reverse micelles, and on the other hand, difference from the chemical methods based on the application of biological reducing agents in aqueous solutions. In the oral presentations and publications, usually the reduced form is used, namely the «biochemical synthesis», with the corresponding explanations on the principles of this method, if necessary.

In this chapter, we present a brief account of the principles of this method, followed by the necessary information on the peculiarities of experimental procedure. Then, synthesis of silver, gold, and copper nanoparticles is described, with the relevant data on the optical spectra and particle sizes.

### 2.1 Prerequisites of the Method

To provide a more complete notion of the biochemical synthesis, we begin with a brief description of the flavonoid properties as well as of the internal medium of reverse micelles, because the combination of these two factors is the main feature of

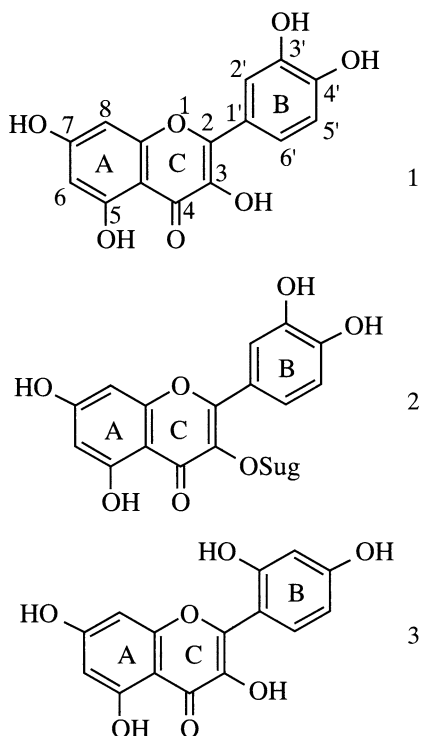
the method and forms the ground for various applications of stable metal nanoparticles in solutions.

### 2.1.1 General Information on the Properties of Flavonoids

Plant pigments of the flavonoid group are low-molecular polyphenolic compounds with structure formed by the three rings: two aromatic rings (A and B) connected by heterocycle (C), which contains oxygen and is referred to also as pyrane ring. As an example, structure of the three flavonoids used by us is shown in Fig. 2.1.

In nature, flavonoids are present in fruits, berries, vegetables, nuts, herbs, and flowers; some drinks are often mentioned as sources of flavonoids, especially tea and red wine (see [248, 249]). Many of these compounds are strongly colored, and this is the origin of bright and diverse coloration of flowers and other plant parts. For the time being, their function in the plant organisms is not fully elucidated [250]. It is known that they can protect cell photosynthetic system from the destructive action of short-wavelength UV radiation and also preserve the plants from various morbidic affections. There exists a great number of flavonoids (more than 4000), divided into subgroups, that differ by the number and location of substituents (hydroxy groups) at various carbon atoms (mainly 3, 5, 7, 3', 4', 5') and by the presence (or absence) of oxygen with double bond at the 4th carbon atom [248–250].

**Fig. 2.1** Structure of flavonoid molecules used in the biochemical synthesis. 1 quercetin; 2 rutin; 3 morin. Sugar is disaccharide that consists of rhamnose and glucose residues. This figure and figs. 2.2, 2.3, 2.13–2.20 were reprinted from *Advances in Nanotechnology*, vol. 11, “Biochemical synthesis, optical properties and sizes of gold nanoparticles”, pp. 119–146, Copyright 2014, author E.M. Egorova, with permission from Nova Science Publishers



In the method of biochemical synthesis, three flavonoids are used from the flavonol subgroup: quercetin, rutin, and morin. They are the powders (crystallohydrates) of yellow color, produced mainly from the peel of onion or from citric plants, where they are present in relatively large amounts.

Like many other flavonoids, these substances are known for their ability to chelate metal ions, as well as for the high and versatile biological activity. For example, quercetin and rutin belong to the vitamin P group and are used in medicine for a long time as a means for the reduction of capillary permeability of blood circulatory system; also, their anti-inflammatory, antioxidant, radioprotective, and antimutagenic properties are widely recognized. The important advantages of these substances are their low toxicity for a human organism and wide spectrum of medicinal effects. There is voluminous literature devoted to the investigation of mechanisms underlying the action of these flavonoids. In the last years, much attention is paid to the research of their interaction with animal cells *in vitro* (including the cells of immune system, muscular and neural cells, and tumor cells) [264] that offer opportunities for the application of these substances as hepatoprotective agents, for combating cancer and a number of other diseases.

According to the literature data, quercetin is studied more intensively than the other two flavonoids under question. This is probably connected with its more significant consumption by a human organism with food products, and hence, studies on the mechanisms of its action are more urgent [255, 259, 260, 262]. Therefore, its interaction with lipoproteins, nucleic acids, various enzymes, and other proteins was the subject of thorough investigations by a number of laboratories [252, 255, 259, 264].

As noted in literature [260, 265], polyphenolic structure of quercetin makes it extremely sensitive to the variations of composition and structure of the environment. It is obvious that biological processes with participation of quercetin and the other biologically active substances proceed in a living organism in the organized medium, in conditions that differ significantly from those which exist in aqueous solutions *in vitro*, where, up to the present time, the vast majority of experiments were performed. Only recently, the publication appeared devoted to the interaction of quercetin in aqueous solution with direct micelles from anionic or cationic surfactants [265], considered as a model of plasma membrane or cell organelle, suitable for the studies of the influence of biological organization on antioxidant activity and other properties of flavonoids. In our opinion, the reverse micellar system is more interesting from this point of view because, as shown below, properties of the internal medium of reverse micelles are more similar to those of the internal media of biological vesicles or cellular compartments in the living organisms. However, as far as we know, no attempts have been undertaken so far to study biologically interesting reactions in reverse micelles with participation of quercetin and other flavonoids.

Thus, by choosing flavonoids as reducing agents, we became pioneers in the studies of the flavonoids interaction with metal ions in reverse micelles. According to the purpose of our work, the main task was to determine the conditions that allow the formation of metal nanoparticles.

### 2.1.2 AOT/Isooctane Reverse Micelles

As already mentioned above, in this case the nanoparticle formation is the result of reduction of metal ions to atoms and further aggregation of atoms and ions in the internal medium of reverse micelle. Properties of this internal medium, or water core, primarily depend on its size, which is determined by the hydration extent  $w = [\text{H}_2\text{O}]/[\text{SAS}]$ . A brief account of the general information on the water properties in micellar core is given in Chap. 1 (Sect. 1.3.4).

The anionic SAS used by us—*aerosol-OT* or AOT—is most frequently applied for the preparation of reverse micellar systems, because it is highly soluble in many nonpolar solvents and allows to obtain stable reverse micelles in a wide range of SAS concentrations and hydration extents. Also, AOT has a unique capacity for binding a large amount of water (up to 10 water molecules per one SAS molecule) without addition of other cosolubilizers. According to the author of [139], this is conditioned by the high flexibility of the AOT molecular structure. Structure of a reverse micelle in  $\text{H}_2\text{O}/\text{AOT}/n\text{-alkane}$  system used in our research is shown in Fig. 2.2 in the general terms.

Formal length of the hydrocarbon part of AOT molecule (at the maximal extension of hydrocarbon tails) is equal to 8–9 Å [136, 139]. Usually, the actual length of this part in micelle is less due to the «bending» of hydrocarbon tails. The main parameters of AOT/isooctane water micelles reported in literature for several hydration extents are presented in Table 2.1. As seen from the table, water micelles have sizes in the range 3–7 nm. The experimental values of hydrodynamic radius found by dynamic light scattering (DLS) technique [137, 139]) are in good agreement with the corresponding theoretical results calculated from the empirical expression proposed in [142]. Hence, this expression may be applied for the estimation of micelle size for the other  $w$  values in the range  $0 < w < 10$ . Size of the aqueous core varies approximately in the range of 2–4 nm; the «binded» water layer thickness lies within 3–5 Å from the polar heads boundary [139] and is increasing with the decrease of hydration extent, reaching its maximum value at  $w < 4$ . It is clear therefore that, at so small hydration extents, all the water in micellar core is «binded» with all characteristic features mentioned above. For example, in AOT/isooctane reverse micelles with  $w = 3.7$ , that are often used in biochemical synthesis, microviscosity inside the water core is 200 times higher than that of bulk water [133]. It is exactly in this medium that synthesis of metal nanoparticles takes place in our case.

Since the biochemical synthesis is based on electron transfer from the flavonoid to metal ion, one can expect the manifestations of the features of electron transfer reactions that proceed in reverse micelles at small hydration extents. The results obtained in studies of various reactions of the same type in reverse micelles [126, 133, 141] indicate that electron behavior in the internal cavity of reverse micelles differs essentially from that in the aqueous solution. As was mentioned already in Chap. 1 (Sect. 1.4), solvation of the electrons generated by pulsed radiolysis in AOT reverse micelles in isooctane depends on the hydration extent: The smaller is  $w$ , the lower is the rate of solvation, and for  $w < 5$ , the electrons are not solvated at

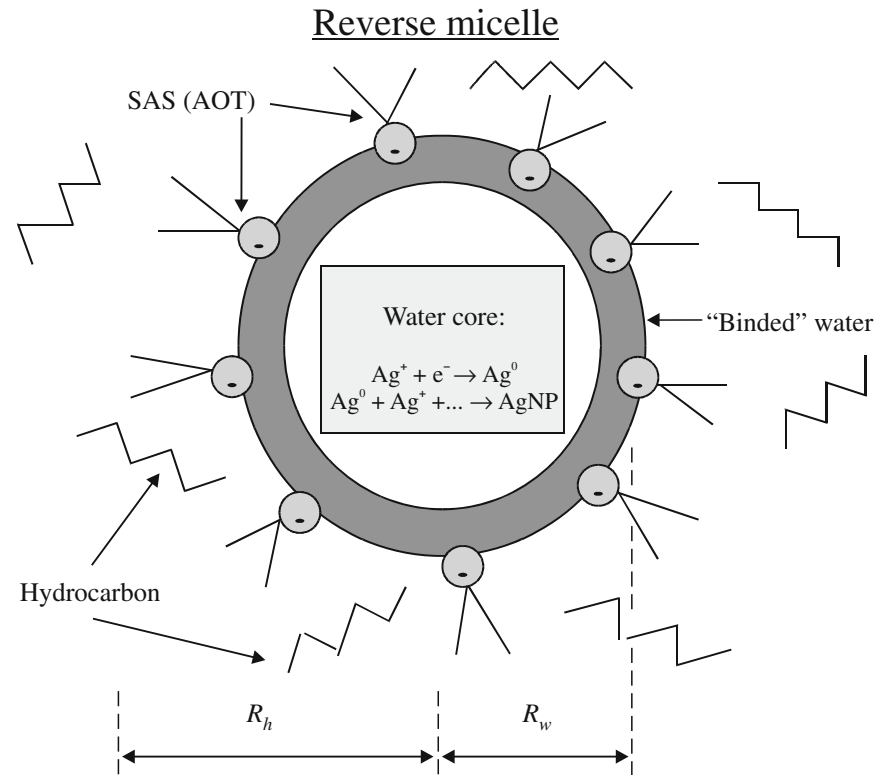


**Fig. 2.2** Structure of AOT reverse micelle in hydrocarbon (in our case, usually in isooctane).  $R_h$  and  $R_w$  are hydrodynamic radius and water core radius, respectively. Reduction of metal ions in the water core is illustrated on  $\text{Ag}^+$  ion as an example. See text for more details

**Table 2.1** Parameters of reverse micelles in water/AOT/isooctane system

$w$	$R_h$ (Å)	$R_w$ (Å)	$N_a$	Reference	$R_h = 1.5w + 16.4$ Å [142]
0	16.4 15 15	9	22 11	[126, 140] [142] [135] [137]	
3.5	~25			[137]	21.65
4	25	10	35	[137]	22
5	~32			[137]	23.9
6	28	14	50	[137]	25.4
8	32	16 19 18	72 115 95	[139] [126] [126]	28.4
9	~36			[137]	29.9

$R_h$  hydrodynamic radius;  $R_w$  water core radius;  $N_a$  aggregation number

all [133, 266]. It was found also that in reactions with electron transfer from aqueous to hydrophobic phase proceeding in AOT reverse micelles, the bound water at the polar heads layer boundary plays an essential role [141]. As will be shown below (Sects. 2.3 and 2.4, Chap. 3), specific properties of the internal medium of reverse micelles, including the influence of bound water, manifest themselves also in the biochemical synthesis of metal nanoparticles.

## 2.2 General Scheme of the Synthesis

General principle applied in the nanoparticle synthesis in reverse micelles consists in mixing the micellar solution of metal ions with that of reducing agent (see Chap. 1, Sect. 1.3.4). In our case, this principle is implemented by mixing separately prepared micellar solutions of flavonoid and metal salt. Micellar solution of flavonoid is prepared with the use of its concentrated solution in ethanol or propanol. It turned out, however, that, apart from this conventional variant, another route also exists, namely injection of aqueous metal salt solution directly into the flavonoid micellar solution. In this case, micellar solution of flavonoid is prepared by solubilization of the flavonoid taken as dried powder in AOT/liquid hydrocarbon (n-alkane) solution. In both cases, the final products are nanoparticles in the water core of micelles and oxidized flavonoids. For each metal, special work was needed in order to select the conditions (concentration of reagents, hydration extent, metal salt composition) that ensure the high rate of formation and stability of nanoparticles, as well as high enough degree of transformation of the metal ions into nanoparticles. According to the observations made on the initial stage of work on biochemical synthesis, as a rule, with the conventional method, the rate of formation and yield of nanoparticles were lower compared to those obtained with the second route, so afterward the nanoparticles were prepared almost exclusively by the latter way. Owing to the peculiarities of optical properties inherent both to the complexes of flavonoids with metal ions and to the nanoparticles, process of nanoparticle formation is accompanied by the characteristic changes of color, thus allowing a visual control of the onset and (approximately) of the rate of synthesis.

## 2.3 Peculiarities of the Experimental Procedure

Whereas our method has some differences from the conventional procedure followed in the nanoparticle synthesis in reverse micelles, prior to the description of examples of the nanoparticle synthesis, we found it reasonable to give the necessary information on the most essential peculiarities of this experiment. Here belong (1) preparation of the flavonoid micellar solution, (2) determination of the flavonoid extinction coefficient in micellar solution, and (3) determination of the stabilizer (AOT) concentration in the water nanoparticle solution obtained from their micellar

solution. Below in this section, we present a brief description of the procedures used in the preparation of the flavonoid micellar solution and estimation of its extinction coefficient; determination of the AOT concentration in water solution of the nanoparticles will be elucidated in Chap. 4 devoted to the preparation of metal nanoparticles in water solutions.

### ***2.3.1 Preparation of the Flavonoid Micellar Solution***

Micellar solutions of flavonoids are prepared by the procedure described in [202, 267, 268]. At first, AOT solution in liquid hydrocarbon is prepared; hexane, heptane, octane, isooctane, and decane can be used as solvents [269]. Experience has shown, however, that isooctane is the most suitable for the nanoparticle synthesis, both from methodological and economical point of view. Then, flavonoid (taken as powder) is solubilized in the AOT solution. The AOT concentration in isooctane lies in the range 0.1–0.3 M, depending on the metal used for the nanoparticle synthesis. In our standard synthesis procedure, the AOT concentration is 0.135 M. For applications that require the lower AOT concentration in micellar or aqueous solution, AOT concentration in isooctane can be reduced; however, in such cases, the additional control is necessary, to check the stability and size of nanoparticles in micellar and water solutions, as well as the AOT concentration in water nanoparticle solution.

AOT and flavonoids were preliminary dried to remove the hydration water, if it was necessary. Concentration of the flavonoids in micellar solution was determined from their optical absorption spectra; for this purpose, the corresponding extinction coefficients had been found in separate experiments.

### ***2.3.2 Extinction Coefficient Determination for the Flavonoids in Micellar Solution [268]***

Similarly to their water–alcoholic or water solutions, micellar solutions of the flavonoids used in our work have two main adsorption bands in the UV region (Fig. 2.3): band I and band II positioned at 360–380 and 240–270 nm, respectively. The absorption bands stem from the  $\pi$ – $\pi^*$  transitions in the two chromophore systems: band I—in the B ring conjugated with three-carbon fragment of the C ring, band II—in the A ring conjugated with the C ring. The corresponding resonant structures for quercetin as an example are shown in Fig. 2.4 [265, 270].

Comparison of absorption spectra of quercetin (Qr) in aqueous solution (phosphate buffer) and in micellar solution in AOT/isooctane revealed different behavior of the two main bands: absorption in the short-wavelength band II was almost the same in the two solutions, while intensity of the long-wavelength band I in micellar solution was significantly higher than in the aqueous one.

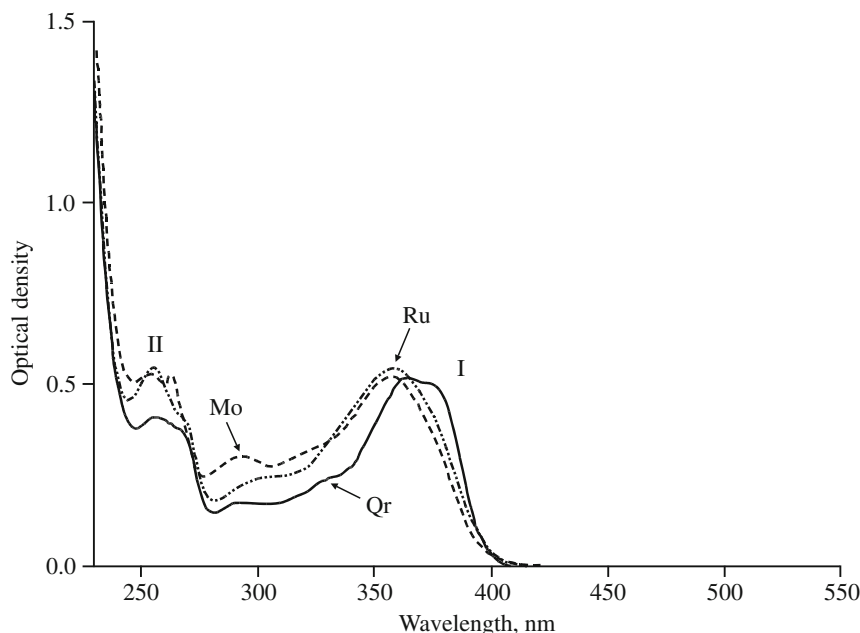


**Fig. 2.3** Optical absorption spectra of flavonoids—quercetin (Qr), rutin (Ru), and morin (Mo)—in micellar solutions. I and II—two main absorption bands. Spectra shown here and in the other figures within this part of the book were measured in 1-mm cuvettes

An example for the 50  $\mu\text{M}$  Qr solution is shown in Fig. 2.5a. Picture of such kind is observed for various quercetin concentrations in the range studied (25–100  $\mu\text{M}$ ). Thus, it turned out that different parts of the flavonoid molecule have various degrees of sensitivity to the changes in external conditions; namely, A ring demonstrates a weak reaction, while B ring reacts significantly stronger.

Hence follows that Qr molecule is positioned inside reverse micelle in such a way that surroundings of the A ring are less different from those in aqueous solution than surroundings of the B ring. Because of its structure, the molecule cannot be located in the region of AOT hydrophobic tails, but only in the polar part of micelle, in the layer of AOT polar headgroups, on its boundary with the polar core or inside the polar core. Since polar core is the most similar in structure to the water solution, the A ring is likely to be located in the polar core (or at least is oriented toward it), and the B ring is located in the region with more rigid structure—in the layer of AOT polar headgroups or on its interface with the polar core.

Owing to the closeness of absorption values in the band II maximum ( $D_{\text{max}}^{\text{II}}$ ) for water and micellar solutions with equal Qr concentration, it is possible to use these values for the determination of Qr extinction coefficient ( $\epsilon$ ). The  $\epsilon^{\text{II}}$  values in series of 8–10 experiments were found from the expression  $\epsilon^{\text{II}} = D_{\text{max}}^{\text{II}}/C_{\text{Qr}} \cdot l$ , where  $C_{\text{Qr}}$



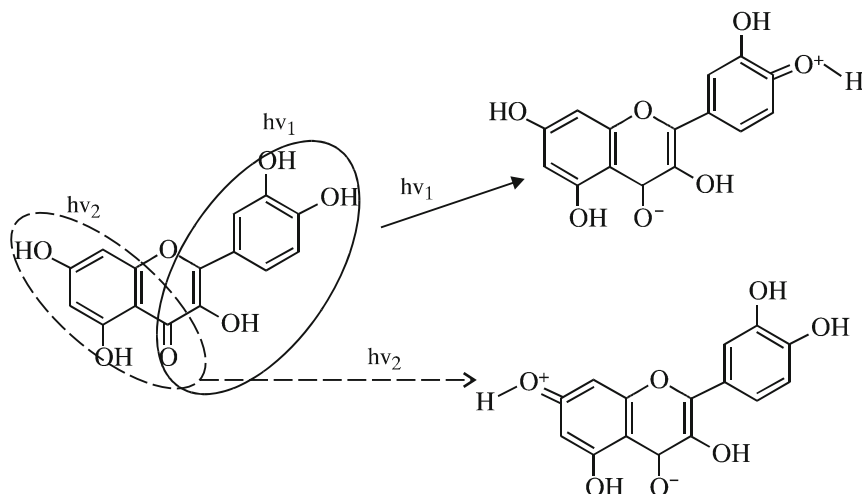


**Fig. 2.4** Resonance structures in quercetin molecule corresponding to the band I ( $h\nu_1$ ) and band II ( $h\nu_2$ ) in optical absorption spectrum [261, 270]. Reprinted from Ref. [261]. Copyright 2006, with permission from Elsevier

is quercetin concentration and  $l$  is optical path length. For water and micellar solutions, they were equal to  $(1.79 \pm 0.07) \times 10^4$  and  $(1.81 \pm 0.08) \times 10^4$  L/mol cm, respectively. Hence, the average value is  $\varepsilon^{\text{II}} = (1.8 \pm 0.1) \times 10^4$  L/mol cm.

Using this extinction coefficient, we compared further the spectra obtained for micellar solutions with constant quercetin concentration and different water content. Figure 2.5b shows the spectra obtained for 50  $\mu\text{M}$  Qr solutions, prepared by solubilization of Qr powder in anhydrous AOT solution in isooctane (curve 2) and in AOT solution in isooctane with preliminary added water, with  $w = 20$  (curve 1). It is seen that absorption in the band I for anhydrous («dry») solution is significantly higher than that for the water-containing solution. These two cases differ in that micelles containing quercetin are formed by AOT molecules with different hydration of the polar heads, so it is possible to assume that electron transitions in the B ring of quercetin suffer a strong influence of the water molecules binded with AOT polar headgroups. It is possible, therefore, that this part of quercetin molecule in the «dry» micelle is located in the AOT polar headgroups layer and forms with them hydrogen bonds through its OH groups and molecules of the binded water.

In Qr micellar solution with the given water content (with the given AOT hydration extent), absorption in the band I depends only on the flavonoid concentration, and hence, one can single out two extinction coefficients determined from the absorption in band I and band II— $\varepsilon^{\text{I}}$  and  $\varepsilon^{\text{II}}$ , respectively. In the particular case of «dry» solution, the extinction coefficient in band I is maximal and equal to  $(2.8 \pm 0.1) \times 10^4$  L/mol cm. At the small hydration extents, ( $w = 3\text{--}5$ )  $\varepsilon^{\text{I}} = (2.26 \pm 0.07) \times 10^4$  L/mol cm.

Extinction coefficient for rutin was determined from spectrophotometric measurements of micellar solutions with several rutin concentrations. These solutions

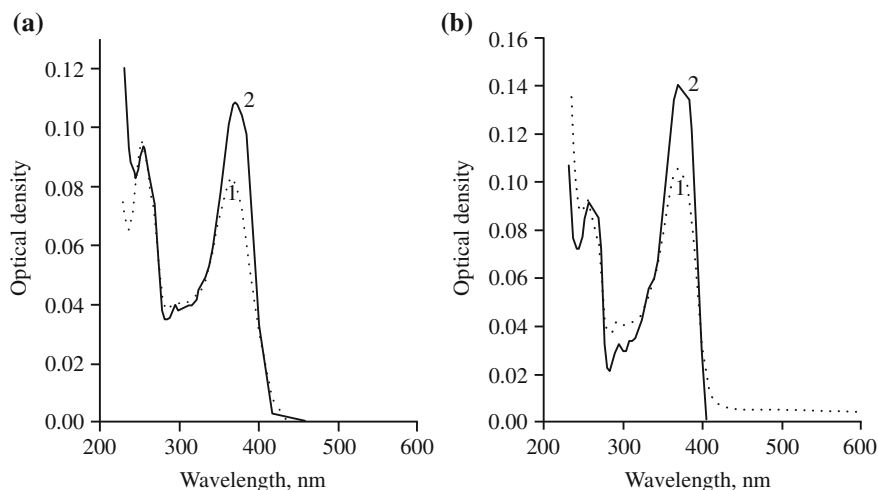


**Fig. 2.5** Spectra of 50  $\mu\text{M}$  Qr solutions in various media: **a** 100 mM sodium phosphate buffer (1) and micellar solution obtained by the introduction of Qr solution in isopropanol into AOT solution in isooctane (2); **b** Micellar solutions obtained by Qr solubilization in isooctane with preliminarily added water to the hydration extent  $w = 20$  (1) and in the “dry AOT solution in isooctane” (2)

were prepared by the introduction of rutin alcoholic solutions into the AOT solution in isooctane; the alcohol concentration in micellar solution did not exceed 1 %. From the results of 5 independent measurements, the extinction coefficients for band I (366 nm) and band II (258 nm) were found to be  $(2.32 \pm 0.13) \times 10^4$  and  $(3.26 \pm 0.33) \times 10^4$  L/mol cm, respectively.

## 2.4 Examples of the Nanoparticle Synthesis

Aqueous solutions of metal salts were prepared on deionized water obtained from the device «Vodoley» (production of «Chimelectronica», Moscow). For the preparation of complex salts (silver diammine nitrate, copper tertammine nitrate, and salts of other metals), 10 or 27 % ammonium hydroxide solutions were added to the metal salt solution (for details see [28]).

Addition of metal salt water solutions to the micellar solutions of flavonoids, after shaking for several minutes, leads to the drastic changes in color and absorption spectra of these solutions that reflect different stages of flavonoids interaction with metal ions, which is completed by the formation of nanoparticles. Synthesis of nanoparticles was performed mainly in the quercetin solutions; also, the experiments with all three flavonoids were conducted to study the effect of differences in their structure on the nanoparticle formation process. Measurements of absorption spectra were performed on the spectrophotometers Helios-a (production of Thermo Electronics, Great Britain) or Shimadzu UV-2600

(Shimadzu, Japan). Particle sizes in solution were characterized by the dynamic light scattering (DLS) technique (known also as photon correlation spectroscopy, PCS) on the devices Horiba LB-550 (Horiba, Japan) or ZetaPALS (Brookhaven Instruments, USA). Electron microphotographs were obtained by means of the transmission electron microscope LEO912 AB OMEGA (Carl Zeiss, Germany). Materials for the microscopy were prepared immediately before the measurements, by placing a drop of solution on the copper grid with preliminary deposited polymer film. The microphotographs obtained were used for plotting the size distribution histograms; the number of particles for each sample was no less than 350.

The biochemical synthesis allows to prepare the micellar solutions of silver, gold, copper, zinc, cobalt, and nickel nanoparticles. In the context of this edition, we considered it to be expedient to present the examples of optical spectra and particle sizes obtained for micellar nanoparticle solutions of three metals—silver, gold, and copper. Silver and copper nanoparticles were applied in studies of the biological effects (see Part II), and gold nanoparticles are of interest for the comparison of their characteristics with those of the nanoparticles prepared by the biological reduction in aqueous solution (see Part I, Chap. 4).

### 2.4.1 Silver Nanoparticles

Addition of silver nitrate aqueous solution to the Qr micellar solution, after shaking for 1–3 min, leads to the sudden change of the solution color—from colorless to pale-yellow or red-brown of different intensity, or even almost black, depending on the nanoparticle concentration. In the absorption spectrum, the two Qr bands disappear and appears instead a new band in the visible region with maximum in the range 420–440 nm, typical for silver nanoparticles in reverse micelles (see [152]). This new band increases gradually, and optical density in the band maximum ( $D_{\max}$ ) reaches its maximum value ( $D_{\max}^0$ ) in 1–4 days; the rate of this increase and the  $D_{\max}^0$  value depend on the chosen parameters of the system (silver salt composition, reagents concentration ratio, etc.). During the next weeks, the deviation from  $D_{\max}^0$  does not exceed 10 % so this value of  $D_{\max}$  is usually considered as corresponding to the stationary stage or completion of the process of nanoparticle formation. Figure 2.6 shows the characteristic form of absorption spectrum registered for the micellar solution of silver nanoparticles on the stationary stage. The intense color of such a solution is retained for a long time (up to several years), thus making possible the visual control of the nanoparticle stability. As an illustration, Fig. 2.7 shows the appearance of micellar solutions with different concentrations of silver nanoparticles.

The rate of formation, yield, and size of nanoparticles depends on several factors, such as silver salt to quercetin concentration ratio, AOT concentration, hydration extent, and silver salt composition; results of the corresponding experiments will be described in Chap. 3. Here, we present just one example (Fig. 2.8): the typical change of absorption spectra that reflects the nanoparticle formation kinetics (at all

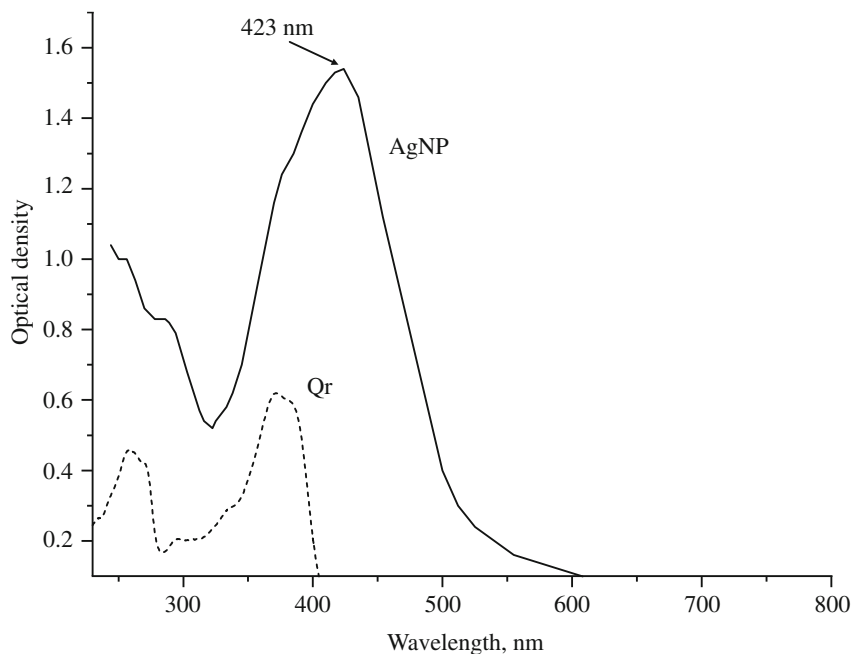
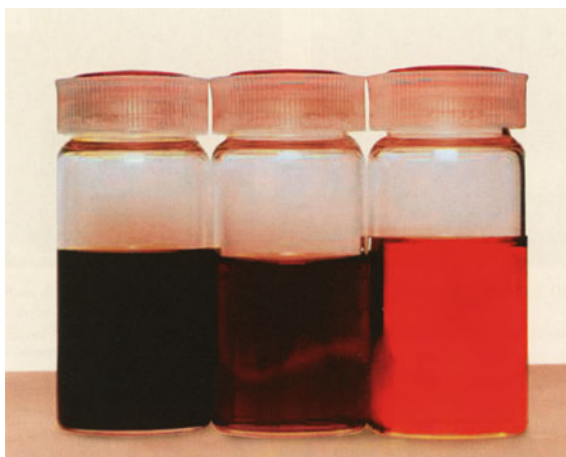


**Fig. 2.6** Characteristic form of the optical spectrum obtained for micellar solution of Ag nanoparticles (AgNP). Reagents concentrations:  $C_{\text{Ag}} = 3 \text{ mM}$ ,  $C_{\text{Qr}} = 0.265 \text{ mM}$ ,  $C_{\text{AOT}} = 0.135 \text{ M}$ ,  $w = 3.7$ . For comparison, spectrum of the initial quercetin solution (Qr) is shown

**Fig. 2.7** Micellar solutions of silver nanoparticles. Nanoparticle concentration decreases from *left to right* (color)



other conditions being equal) observed for different silver salts, namely nitrate and diammine nitrate ( $\text{Ag}(\text{NH}_3)_2 \text{NO}_3$ ). As seen from this Figure, in both cases a well-formed band of nanoparticles can be observed after 30–40 min; however, the rate of the band increase (i.e., the rate of nanoparticle formation) and the  $D_{\text{max}}$  value

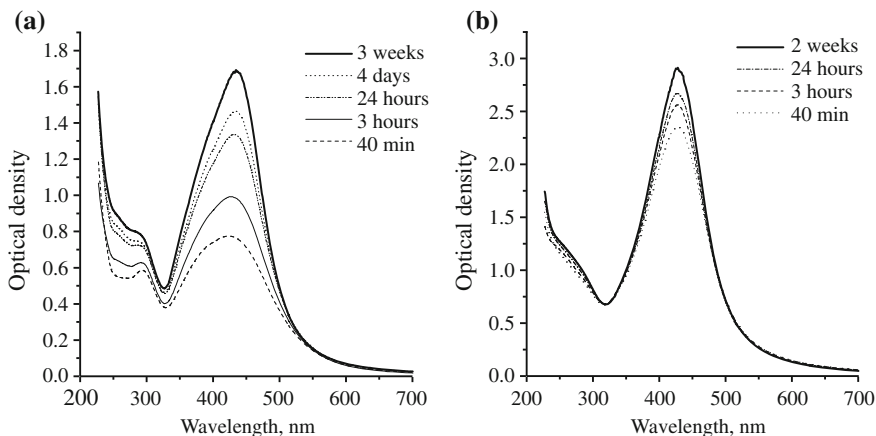


**Fig. 2.8** Formation kinetics of silver nanoparticles from silver nitrate (a) and silver diammine nitrate (b) solutions.  $C_{Ag} = 3$  mM,  $C_{Qr} = 0.236$  mM,  $C_{AOT} = 0.15$  M,  $w = 3.7$ . Insets show the time interval from the introduction of silver salt solution

(which reflects the degree of ion conversion or the yield of nanoparticles) are significantly higher for ammonium salt. This difference is distinctly observed at silver salt concentrations in micellar solution in the range of several millimoles. Our study on the origin of this difference allowed to suggest [28] that it could issue from the significant deviations from ideality in the  $AgNO_3$  water solution introduced into the Qr micellar solution in the course of nanoparticle synthesis. To test the effect of non-ideality of the  $AgNO_3$  solution, optical densities in the nanoparticle band maximum were calculated with correction for the activity coefficient ( $D_{max}^c$ ):

$$D_{max}^c = D_{max}^* \cdot \gamma \quad (2.1)$$

where  $\gamma$  is the activity coefficient, and  $D_{max}^*$  is optical density calculated for the concentrations of silver nitrate in micellar solution by the Bouguer–Lambert–Beer law (see also Chap. 3 below). In other words,  $D_{max}^*$  values for each salt concentration correspond to the maximum possible yield of nanoparticles, or to the degree of conversion of silver ions equal to 1.

The  $D_{max}^c$  values found from Eq. 2.1 (theoretical curve) were compared with experimental  $D_{max}^0$  values obtained experimentally for several silver nitrate concentrations (in the range 0.02–0.3 M) in its initial water solution. The results are shown in Fig. 2.9b. It is seen that there is quite satisfactory agreement with the theory in the whole range studied. For comparison, the  $D_{max}$  dependence on ionic strength of the initial silver salt solution is also shown, calculated for the “ideal case” ( $\gamma = 1$ ), as well as experimental data points obtained for the  $Ag(NH_3)_2 NO_3$  concentrations in its initial solution in the decimolar range. It is clear that (1) significant deviations for silver nitrate begin from 0.1 M and (2) for diammine nitrate there is a good agreement with theoretical results for the «ideal» case.

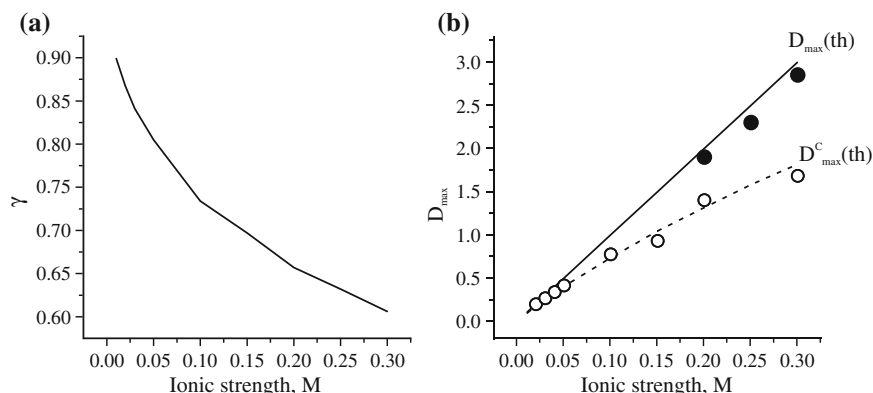


**Fig. 2.9** Manifestation of the non-ideality observed for water solution of silver nitrate. **a** The dependence of activity coefficient ( $\gamma$ ) on  $\text{AgNO}_3$  concentration in water solution calculated from the Debye–Hückel theory [281] in the range 0.01–0.1 M and from the Gibbs–Dughem equation in the range 0.1–0.3 M [282]. **b** Comparison of theoretical (lines) and experimental (dots) dependencies of  $D_{\max}$  at the stationary stage on silver salt concentration in the initial solution. Solid line refers to the ideal solution ( $\gamma = 1$ ), dashed line—to the solution where  $\gamma$  varies as shown in (a). Points ○—nitrate, ●—diammine nitrate

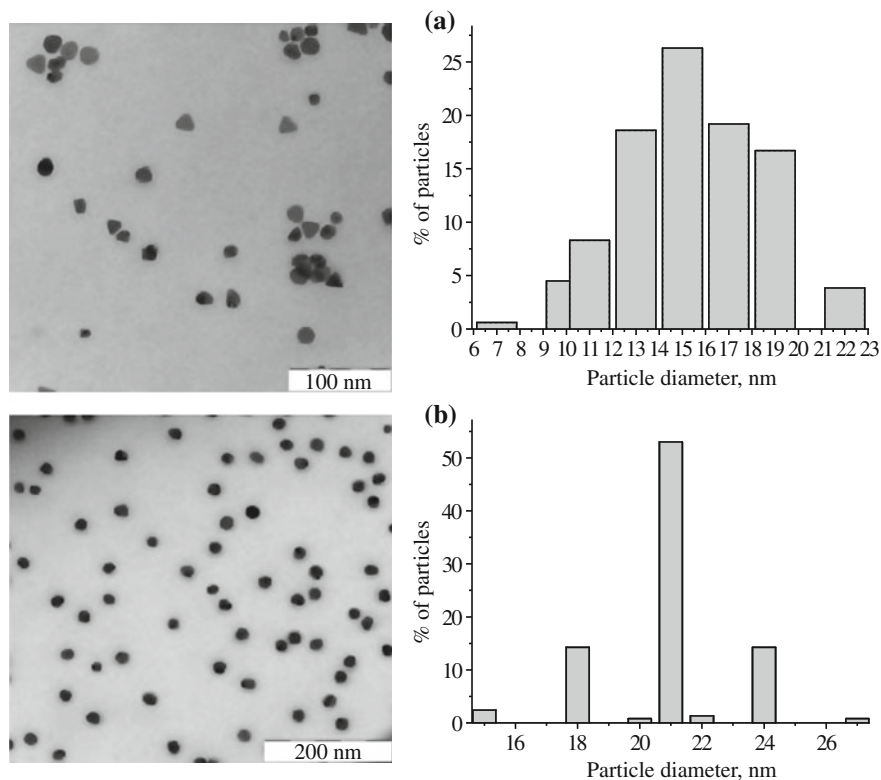
Hence follows that the most probable cause of the acceleration of nanoparticle formation with the use of ammoniac silver salt (for silver salt concentration in the initial water solution,  $C \leq 0.3$  M) may be the increase of effective concentration of the added metal ions due to the difference in activity coefficients of the two tested salts.

In the course of studies on the mechanism of silver nanoparticle formation in micellar solution, the problem arose of determination of the intermediate stages of Qr interaction with  $\text{Ag}^+$  ions. As seen from the adsorption spectra of micellar solutions of silver nanoparticles in the standard biochemical synthesis procedure (see Fig. 2.8), here the quick formation and increase of the nanoparticle band intensity are observed, so that it is impossible to discern the intermediate stages. This problem was solved in studies of the quercetin interaction with silver ions at low concentrations of the reagents [28, 268]. It was shown that at the first stage, the  $[\text{Ag}^+ \dots \text{Qr}]$  complex formation takes place, which manifests itself in the noticeable growth of the 295-nm band, present in the original Qr spectrum as a small «bump» between the two main bands I and II (see Fig. 2.3). Theoretical estimates of the enthalpy of complex formation between quercetin and metal ions [271], as well as our researches on the influence of flavonoid structure on the nanoparticle formation process [28], give grounds to believe that this complex is formed by binding of silver ions with the oxygen atoms located at C3 and C4 atoms in quercetin molecule. Then, this complex dissociates with the formation of the oxidized quercetin and silver atoms; association of silver atoms and ions leads to the formation of nanoparticles which can be observed in the spectrum by the characteristic band in the range 420–440 nm. Isolation of the band corresponding to the complex and determination of its extinction coefficient will be briefly considered later, along with

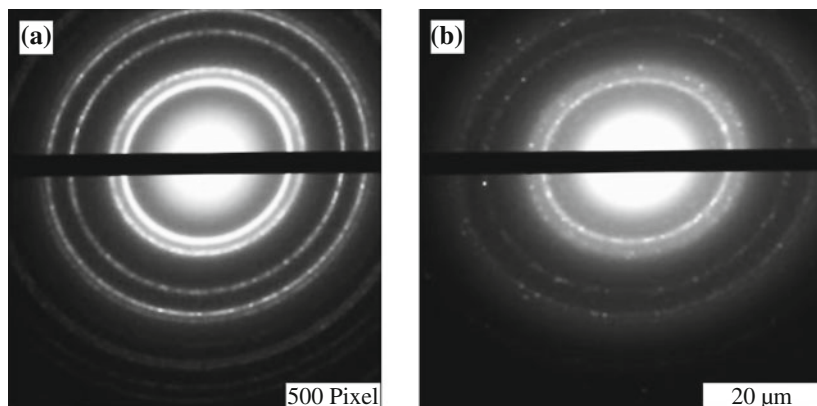
the description of the procedure used for the determination of extinction coefficient of silver nanoparticles in micellar solution (Chap. 3, Sect. 3.1.2).

Figure 2.10 shows electron microphotographs and the corresponding histograms of particle size distribution on the stationary stage (one day after the beginning of synthesis) for the nanoparticles prepared from silver nitrate and silver diammine nitrate with the equal initial salt concentration and hydration extent. It is seen that the nanoparticles produced have different size: In the Gaussian approximation, the average size is 15 nm for nitrate and 21 nm for ammoniac salt.

Analysis of electron diffraction patterns shows that nanoparticles have a crystal structure with lattice parameters close to those of gold crystals. Example in Fig. 2.11 shows the diffraction patterns for the crystal gold sample (a) and silver nanoparticle preparation obtained from the ammoniac salt (b). It can be seen that diffraction patterns are practically identical; less clear image in the case of nanoparticles is explained by much lower density of the metal. Silver nanoparticles may have different shapes: In the case of ammoniac salt, the shape is approximately



**Fig. 2.10** Electron microphotographs and size distribution histograms for the nanoparticles (on the stationary stage) obtained from nitrate (a) and diammine nitrate (b) at silver salt concentration 3 mM and  $w = 3.7$



**Fig. 2.11** Electron diffraction patterns for the standard sample of bulk gold (a) and for the silver nanoparticles obtained from ammoniac salt (b)

spherical, whereas in the case of silver nitrate, also triangles and hexagonal particles are formed (Fig. 2.10).

According to our observations, this difference is connected not with the metal salt composition but rather with the different rate of nanoparticle formation: in the case of diammine nitrate, reduction of the rate of nanoparticle formation also leads to the appearance of crystalline particles of different shapes. It should be noted also that comparison of the electron micrographs obtained for one and the same solution at different times from the beginning of synthesis can detect changes in the average size and shape of nanoparticles. These changes probably reflect the crystallization processes, as well as nanoparticle aggregation and dissociation of these aggregates occurring in the system until the equilibrium is established.

Example of a histogram obtained by PCS for micellar solutions of silver nanoparticles is shown in Fig. 2.12. Measurements give a single peak with the average size in the range 10–26 nm; the peak position depends on the nanoparticle

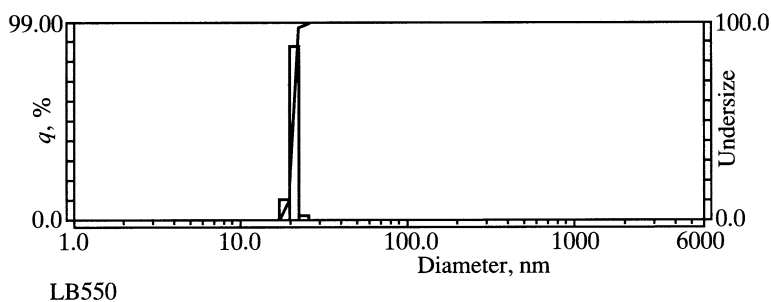


**Fig. 2.12** Typical particle size distribution in micellar solution of silver nanoparticles measured by PCS technique with the help of Horiba LB-550. Average particle size—20.3 nm



concentration in solution. Similar result for these solutions was obtained on the device Zetasizer Nano ZS (manufactured by Malvern, Great Britain), which also implements the PCS method.

Comparison with TEM data indicates that, as a rule, measurements by PCS in solution give the average nanoparticle size somewhat greater than that obtained by electron microscopy. As will be seen later, the same is observed in the size measurements of gold nanoparticles. Discussion of the possible reasons of such discrepancy is given in the following section.

### 2.4.2 Gold Nanoparticles

Changes in the spectra of Qr micellar solutions after the addition of  $\text{HAuCl}_4$  (also referred to below as golden acid, GA) depend on the Qr/GA molar ratio. Here, we give examples of the results obtained with the excess of Qr (in the range  $1 < \text{Qr/GA} < 2.5$ ) and then with the equimolar ratio of reagents or with the excess of GA ( $0.25 < \text{Qr/GA} < 1$ ).

At the excess of Qr, addition of  $\text{HAuCl}_4$  water solution leads to the rapid changes in the color of solution. First bright-red (rather ruby) color appears and then (in 1–2 min) the color acquires the purple tint; its intensity increases in the subsequent 10–15 min. Afterwards, no color changes take place and such a red-purple solution remains stable for a long time (up to several years).

Photograph of the red-purple solutions is shown in Fig. 2.13. Typical changes of the optical spectra at the Qr excess are shown in Fig. 2.14. In the first several minutes, the band I of quercetin decreases and simultaneously the increase of band 295 nm and appearance of the weak band in the visible region are observed, in the range 535–540 nm. Band II suffers practically no changes. In the subsequent 15–30 min, band I continues to decrease and finally disappears, and the two other bands become more intense, the band in the visible region acquiring a distinct maximum at 537–540 nm. This latter band lies in the well-known region characteristic for the absorption of colloidal gold, between 500 and 540 nm, depending on the particle size [46, 48, 128, 228].

This band suffers insignificant changes in the next 2–4 days and then remains unchanged and reproducible for several years. However, its intensity is low compared with that observed for the silver nanoparticles: Usually,  $D_{\text{max}}$  does not exceed 0.24–0.26 for the measurements in 1 mm cuvette. Similar spectra changes take place after the addition of  $\text{HAuCl}_4$  to morin micellar solution. The only difference is that solubilization of this flavonoid in AOT/isooctane solution goes more slowly, and therefore, additional time is needed to reach the concentration level required for the necessary rate of the nanoparticle synthesis. The spectra changes shown here are similar to those mentioned above in the description of the mechanism of silver nanoparticle formation (see also [268]): On the first stage, the  $[\text{Qr} \dots \text{Au}^{3+}]$  complex is formed, and this event is reflected in the spectrum by the increased intensity of 295 nm band. Then, this complex dissociates with the formation of atomic  $\text{Au}^0$



**Fig. 2.13** Photograph of the gold nanoparticles in micellar solutions. Concentration increases from *left to right*

and oxidized Qr. Metal atoms play a role of «seeds» for the subsequent nanoparticle formation by means of the association of metal atoms and ions. As in the case of silver, the complex may be formed through the coherence of metal ions with oxygens at C3 and C4 atoms. Also, the probability exists of the ions binding with oxygens at C4 and C5 atoms. The latter version issues from the estimates of (1) enthalpies of the Qr complexes with metal ions and (2) sizes of the cavities between the oxygen atoms at C3–C4 and C4–C5 positions [271].

If GA concentration exceeds that of Qr, the process of nanoparticle formation provokes the spectra changes as shown in Fig. 2.15. Immediately after the addition of  $\text{HAuCl}_4$ , the ruby color also appears and, after 2–3 min, increases the intensity of 295 nm band, indicative of the complex formation. However, the red color quickly darkens, and after 15–20 min, metal is precipitated, and the solution acquires a golden color, characteristic for the  $\text{HAuCl}_4$  solution, testifying to the destruction of both complex and nanoparticles. We regarded this as a consequence of the quercetin incapability of the effective reduction of  $\text{Au}^{3+}$  ions in the acidic medium inside the reverse micelles at the high  $\text{HAuCl}_4$  concentrations used in this case. This problem was solved by the increase of pH; for this purpose, 2–3 min after the addition of  $\text{HAuCl}_4$ , water solution of ammonium hydroxide was added to the system to the concentration 0.01–0.03 M. Addition of  $\text{NH}_4\text{OH}$  leads first to the appearance of the nanoparticle band and that of the gold ions in water solutions (313–315 nm). Hence follows that the solution contains free  $\text{Au}^{3+}$  ions in addition

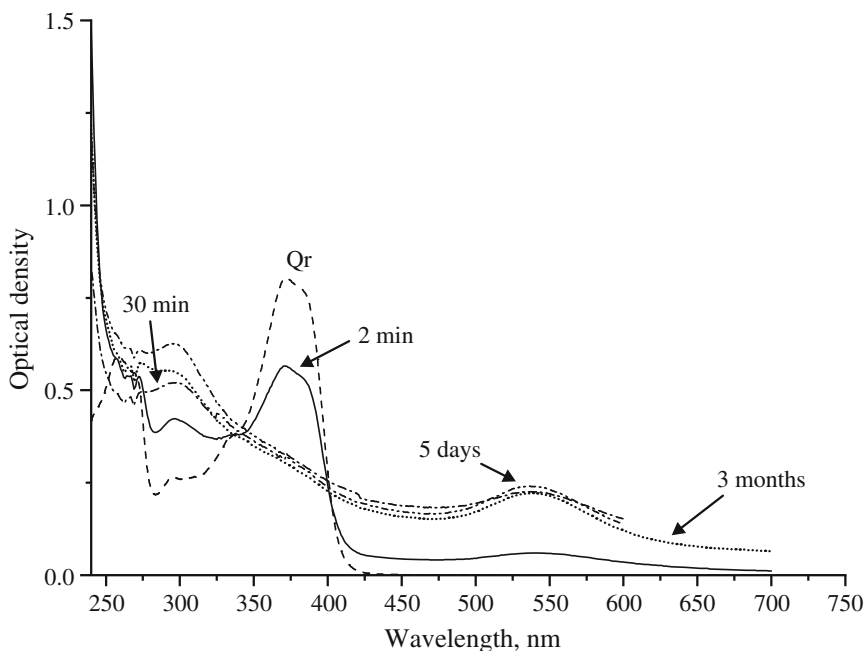


**Fig. 2.14** Gold nanoparticle formation in micellar solution with the excess of Qr. Optical spectra measured in different time intervals after the introduction of aqueous  $\text{HAuCl}_4$  solution.  $C(\text{HAuCl}_4) = 1.55 \times 10^{-4} \text{ M}$ ,  $w = 2$ . Initial Qr concentration— $3.89 \times 10^{-4} \text{ M}$

to those participating in the complex with Qr or transformed into the nanoparticles. After 3–4 h, the  $\text{Au}^{3+}$  band decreases, and at the same time, the band at 537–540 nm increases, showing to the increase of gold nanoparticle concentration. The growth of this band continues for several days (see inset in Fig. 2.15), until the maximum optical density  $D_{\text{max}} = 0.4\text{--}0.5$  is established. Thus, here a higher concentration of nanoparticles is achieved, in comparison with the previous case.

Particle sizes were determined by TEM and PCS methods. Examples of the electron micrographs of Au nanoparticles in micellar solutions are shown in Figs. 2.16 and 2.17. Images shown in Figs. 2.16a and 2.17a are obtained for the nanoparticles synthesized at the excess of Qr and those in Figs. 2.16b and 2.17b—at the excess of GA. The nanoparticles exhibit a wide variety of shapes: hexagonal, pentagonal, triangle, cylindrical, and spherical shapes are present. Relatively small density of the particles per unit area in Fig. 2.16 is accounted for by the dilution of the nanoparticle solution for the microscopy measurements; dilution was necessary to avoid artifacts caused by the high AOT concentration in micellar solution. At the higher magnification (Fig. 2.17), it is seen that particles have rounded corners, but nevertheless some of them undoubtedly look like crystals.

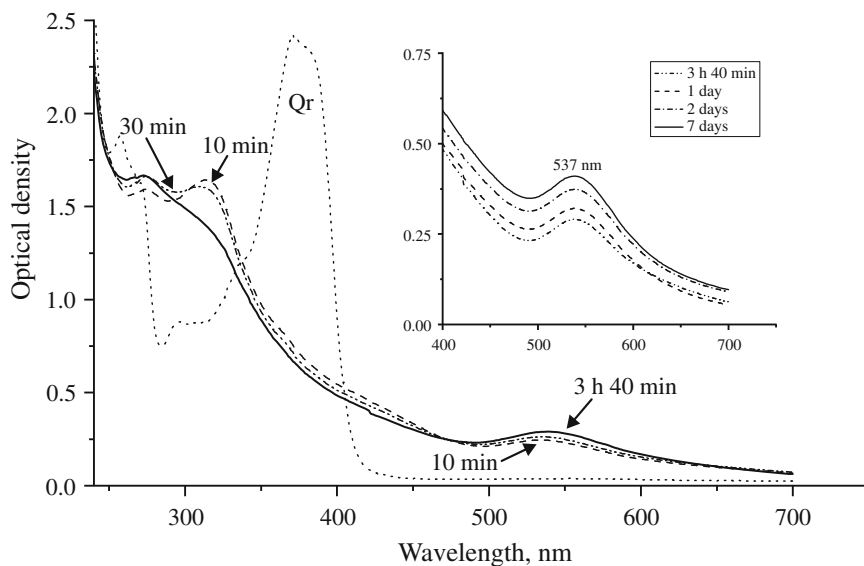


**Fig. 2.15** Gold nanoparticle formation in micellar solution at the excess of  $\text{HAuCl}_4$ . Optical spectra measured in different time intervals after the introduction of aqueous  $\text{HAuCl}_4$  solution.  $C(\text{HAuCl}_4) = 1.944 \times 10^{-3} \text{ M}$ ,  $w = 4$ . Initial Qr concentration— $1.04 \times 10^{-3} \text{ M}$

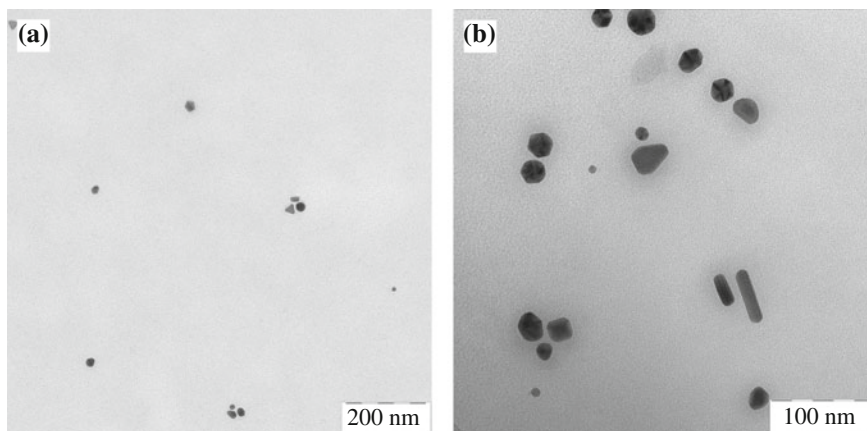


**Fig. 2.16** Electron micrographs of gold nanoparticles at the excess of Qr (a) and at that of GA (b)

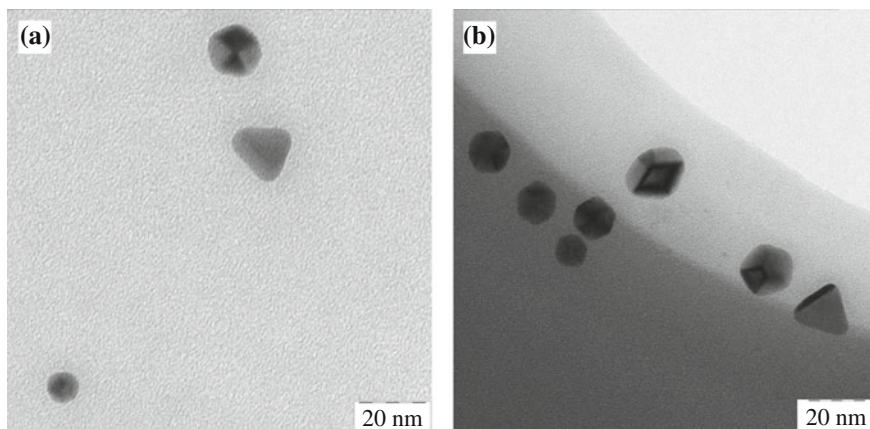


**Fig. 2.17** Electron micrographs of gold nanoparticles at the higher magnification. Excess of QR (a) and excess of GA (b)

The electron diffraction analysis shows that nanoparticles actually have crystal structure with the parameters corresponding to FCC (face centered cubic) structure of the bulk gold. Typical diffraction pattern of the gold nanoparticles is shown in Fig. 2.18a. Comparison with the diffraction pattern of a standard crystal gold sample (Fig. 2.18b) shows that reflexes are practically identical, though for nanoparticles they are less expressed because of the lower density of the substance.

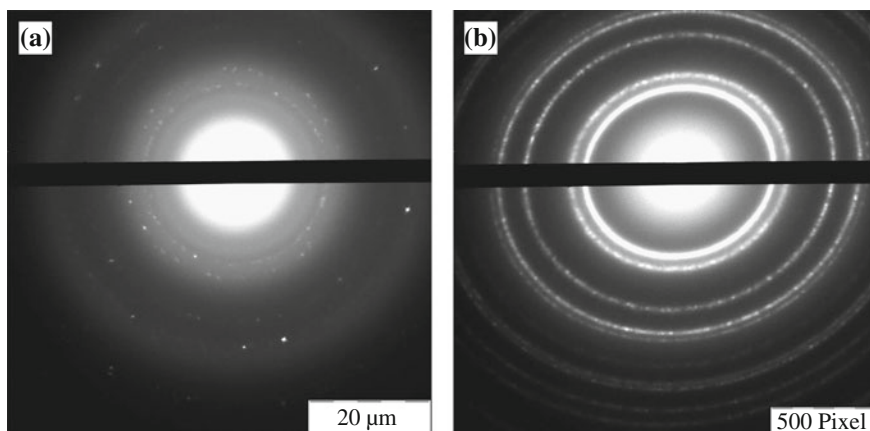


**Fig. 2.18** Electron diffraction patterns for gold nanoparticles in micellar solution (a) and for a standard sample of crystalline gold (b)

Size distributions for the particles produced at the excess of Qr and GA are shown in Fig. 2.19a and b, respectively. In both cases, the majority of nanoparticles (over 80 %) have sizes in the range 7–25 nm. The Gaussian approximation results in the average sizes of  $19.6 \pm 1.3$  nm (Fig. 2.19a) and  $21.5 \pm 5.5$  nm (Fig. 2.19b).

So in both cases, we obtain similar average size of the particles, but the distribution at the excess of GA is somewhat wider than that at the excess of Qr. The data shown above were obtained for the relatively «young» particles (2–4 weeks after the beginning of synthesis). Control of the same solutions by the TEM method in the course of long-term storage had shown that, for both types of solutions, size distribution undergoes similar changes. Examples of the histograms obtained a year after the beginning of synthesis are shown in Fig. 2.20.

For the excess of Qr, we obtain the average diameter of  $16.3 \pm 8.5$  nm (Fig. 2.20a) and for the excess of GA— $20.2 \pm 9.9$  nm (Fig. 2.20b). That is, the average size slightly decreases with time or remains practically constant, while the size distribution becomes significantly wider in both cases. This is probably the consequence of slow processes of the particles association and dissociation taking place in solution.

Another interesting observation may be made concerning the contribution of triangular particles in our micellar solutions. As known from the data available in literature on the biological activity of silver nanoparticles, their toxicity may depend on the particles shape, and there are reasons to assume that triangular particles are more toxic than spherical ones [272]. Also the data exist that indicate to the significant difference in biological activity of the triangular and spherical gold nanoparticles [18, 273]. In view of the possible practical applications of our gold nanoparticles in medicine, we found it useful to evaluate the contribution of triangular nanoparticles and its variation with time.

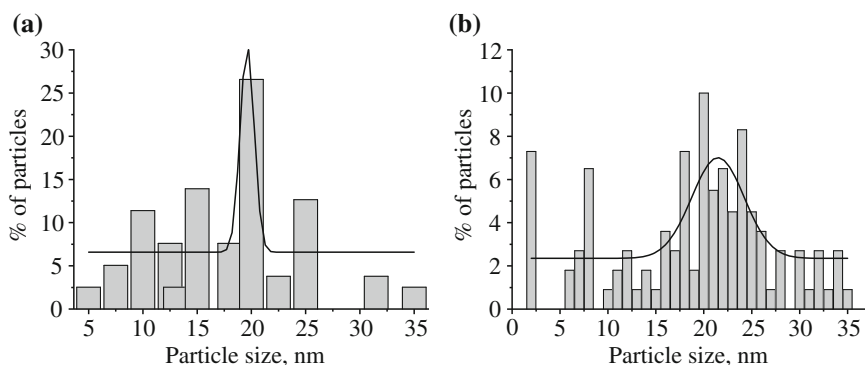


**Fig. 2.19** Particle size distribution obtained from TEM data for the “young micellar solutions of gold nanoparticles at the excess of Qr (a) and at that of GA (b)

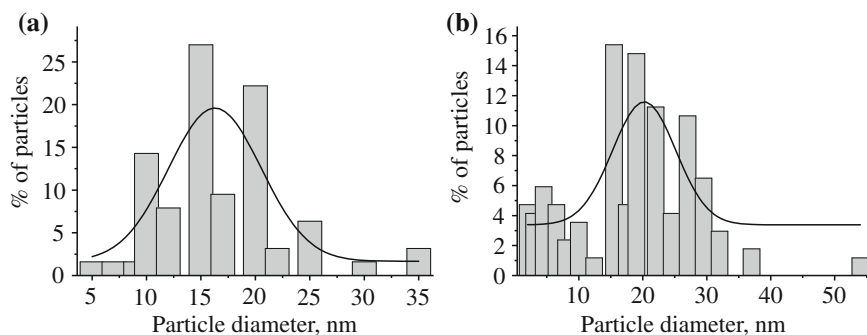


**Fig. 2.20** Particle size distribution obtained from TEM data for the “old micellar solutions of gold nanoparticles at the Qr excess (a) and at the GA excess (b)

It turned out that, for hydration extents  $2 < w < 4$ , the contribution of triangular particles in the micellar solutions depends on the Qr/GA ratio. At the Qr excess (in the range of  $2 < \text{Qr/GA} < 2.5$ ) for the «young» solutions, we obtained significantly more triangles (15–20 %) than at the excess of GA (4–6 % for  $\text{Qr/GA} = 0.5$ ). In our view, this difference is connected with the different rate of synthesis as a consequence of different pH of the medium: at the excess of Qr, synthesis takes place in the more acidic media, where the reduction proceeds slower than at the higher pH resulting from the addition of ammonia solution.

The same reason is likely to be responsible for the diminution of contribution of the non-spherical particles (including triangles) at the basic pH observed in [226] for the gold nanoparticles prepared in water solution by the reduction with plant extract (see Chap. 1, Sect. 1.6). It seems probable, therefore, that it is possible to avoid the formation of triangular nanoparticles by the acceleration of synthesis. This observation may be useful for the preparation of nanoparticles non-toxic for biological objects.

In both types of solutions, portion of the triangular particles decreased with time: After the storage for one year for  $\text{Qr/GA} \approx 2$  and  $\text{Qr/GA} \approx 0.5$ , it was found equal to 7–10 and 2–3 %, respectively. Thus, for the synthesis procedure and solution parameters used in our experiments, a decrease of the triangles' contribution is independent on the ratio of main reagents and acidity of the medium. So it is possible to expect that our «old» preparations will be less toxic than the «young» ones.

Measurements of the particle sizes in solution by PCS method give the results similar to those shown above for Ag nanoparticles. There is also one peak in the histogram, the average particle size is larger than that obtained from the TEM data for the same solution, and this difference is more marked than in the case of silver nanoparticles. A typical histogram for the «young» solution prepared at the excess of Qr is shown in Fig. 2.21. Average size of the particles is equal to 42.1 nm; the standard deviation is 2.5 nm. Comparison with the histogram based on the TEM

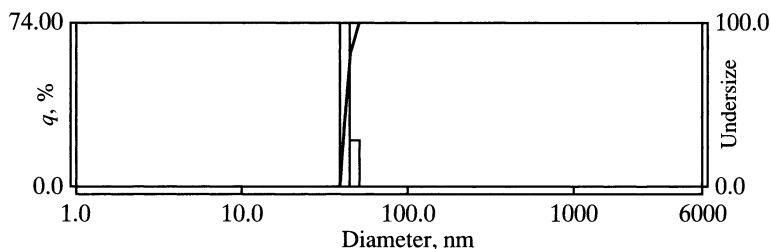


**Fig. 2.21** Particle size distribution obtained by PCS technique for the “young micellar solutions of gold nanoparticles at the excess of Qr. Average particle size—42.1 nm

data (see Fig. 2.19a) shows that the average size and the standard deviation measured by PCS are approximately 2 times greater than those obtained by TEM. The same difference was observed for nanoparticles synthesized at the excess of GA. Similar discrepancy between the PCS and electron microscopy results was detected in [128] for the gold nanoparticles synthesized both in aqueous solution (reduction with citrate) and in reverse micelles (reduction with hydrazine and other non-biological reducing agents).

Such an increase of the average diameter (or hydrodynamic radius) in comparison with the electron microscopy data was observed not only for gold nanoparticles but also for the particles of different nature—liposomes, latexes, and metal oxides [274]. This was assumed to be connected mainly with one of the PCS disadvantages, i.e., its extreme sensitivity to the presence of large particles that scatter light most strongly—as is generally known, the scattering intensity is proportional to  $r^6$ , where  $r$  is particle radius. Therefore, even a small numerical contribution of the large particles can cause a significant increase of the measured average particle size.

In our opinion, apart from the high sensitivity of PCS method to the presence of large particles, the observed discrepancy may be provoked by another cause. Firstly, the error is possible because of the deviation of the true particle shape from spherical one assumed in calculations of a particle hydrodynamic radius by the Stokes–Einstein equation, and secondly, as noted also in [128], the error may happen due to the proximity of the nanoparticle absorption band to the laser beam wavelength (in the device Horiba LB-550 this wavelength is 633.4 nm). In our case, there are two lines of indirect evidence in favor of the latter version: (1) the difference between the PCS and TEM data is greater for gold nanoparticles than for silver ones that could be expected since the absorption band of gold nanoparticles is more close to the laser wavelength and (2) our results obtained on the same device for uncolored solutions which do not absorb in the visible region. For example, for the standard polystyrene latex particles with the size of 20 nm, Horiba LB-550 gives  $18.2 \pm 1.8$  nm, i.e., there is a good agreement for the particles with almost the same average size as that determined for the gold nanoparticles by TEM.

Control of the particle size in micellar solutions for Au nanoparticles in various time intervals after the beginning of synthesis had shown that, unlike the results



obtained by electron microscopy, the average particle size increases with time up to 50–60 nm. Besides, in some cases, the bimodal distribution is observed, where one peak is close to the average size determined by TEM, and the other one lies beyond the nanosized region (exceeds 100 nm). Result of such kind obtained half a year after the synthesis of nanoparticles at the excess of  $\text{HAuCl}_4$  is shown in Fig. 2.22. More than 60 % of the particles have a size in the range 17–23 nm (average 21.6 nm) and approximately 40 %—in the range 170–200 nm. If this is not the consequence of the well-known problems with reliability of the analysis of the autocorrelation function for polydisperse samples (see, e.g., [275]), one can suggest that the larger particles responsible for the discrepancy with TEM data in the «young» solutions gradually aggregate and increase in number, so that they finally appear in the histogram as a separate peak. It should be added that such large particles can be of nonmetallic nature; for example, in our case, aggregates of the AOT micelles may be present, containing (or not containing) Qr or  $\text{HAuCl}_4$ .

### 2.4.3 Copper Nanoparticles

Spectrophotometric studies of the copper ion interaction with quercetin in micellar solutions had shown that, after the addition of aqueous solutions of simple salts (sulfates or nitrates), a bathochromic shift of the Qr band was observed testifying to the complex formation where copper ion is associated with oxygens of the catechol group (binded with C3' and C4' atoms in the ring B, see Fig. 2.1); similar situation takes place in the  $\text{Cu}^{2+}$  ion interaction with Qr and other flavonoids in water or water–alcoholic solutions [257, 262, 264, 276]. Also it is known that, apart from the formation of complexes, in its molecular solutions, Qr can be oxidized with the formation of the products absorbing at the wavelengths 330–335 nm and also of  $\text{Cu}^+$  ions [257, 262]. Further oxidation of quercetin and reduction of  $\text{Cu}^+$  ions to atoms in micellar solution could lead to the nanoparticle formation that can be detected by the appearance of characteristic band in the range of 550–570 nm. It turned out, however, that the process did not proceed further and the nanoparticle formation was not observed. We supposed that the reason was the instability of  $\text{Cu}^+$  ions which did not

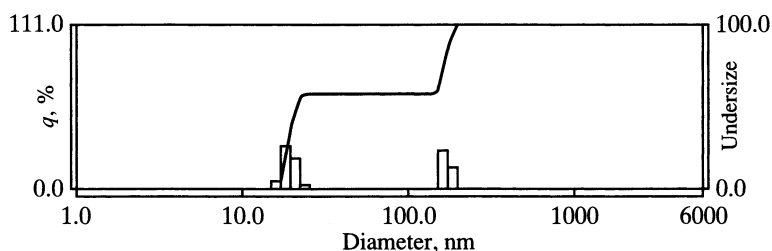


**Fig. 2.22** Particle size distribution obtained by PCS technique for the “old micellar solutions of gold nanoparticles at the excess of GA

allow the complex formation with quercetin, where the reduction to atom could be realized. Similar problem arose, for instance, in studies of metal ion reduction by the hydrated electron in aqueous solution [169, 277], or in the synthesis of copper nanoparticles in aqueous solution in the presence of polymer [278]. In both cases, special efforts were undertaken to stabilize  $\text{Cu}^+$  ions by addition of the agents forming stable complex with these ions.

Following the same logic, and taking in account also that univalent copper ions form stable complexes with ammonia [168, 278], instead of the simple salts, we used ammoniac copper salts obtained by the introduction of ammonium hydroxide into sulfate or nitrate water solutions, resulting in the formation of complex cations  $[\text{Cu}(\text{NH}_3)_4]^{2+}$ . We assumed that, after the reduction of these ions in the complex with quercetin, single-charged cations formed will be stable enough to realize the next stage, i.e., its reduction to atom with the subsequent formation of nanoparticles. Indeed, addition of ammoniac copper salts  $[\text{Cu}(\text{NH}_3)_4]\text{SO}_4$  or  $[\text{Cu}(\text{NH}_3)_4]\text{NO}_3$  to the Qr micellar solution gave rise first to the complex formation and then to the appearance of nanoparticles. These events were reflected in the corresponding changes of Qr absorption spectra in micellar solution. Typical picture observed for the hydration extent 3.7 and ratio  $C_{\text{Cu}}^0:C_{\text{Qr}}^0 \approx 10:1$ , corresponding to the maximum yield of copper nanoparticles, is shown in Fig. 2.23. At first, shift of the band I takes place which indicates to the complex formation; then, this band disappears, and the band appears corresponding to the copper nanoparticles (545–555 nm). The complex dissociates with the formation of the two products: oxidized quercetin (band 320–330 nm) and nanoparticles. The synthesis goes fast enough under standard conditions, so that already in 2 min the band I of original quercetin is not visible, and a weak absorption appears in the band of nanoparticles. As in the case of silver,

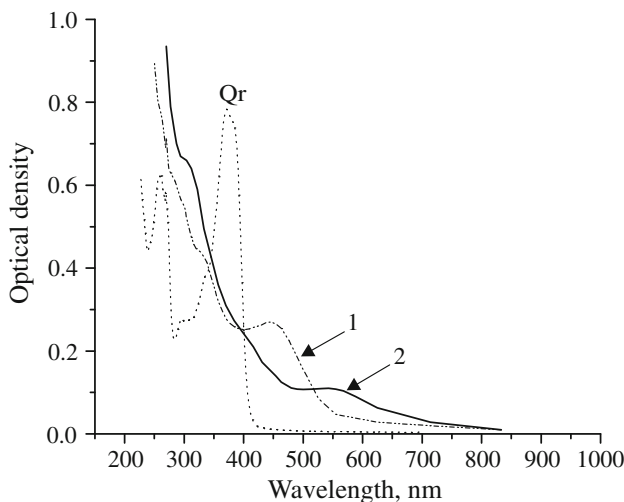


**Fig. 2.23** Spectrum changes of Qr micellar solution in 2 min (1), and 30 min (2) after the introduction of ammoniac copper salt.  $C_{\text{Cu}}^0 = 3.4 \text{ mM}$ ,  $w = 3.7$   $C_{\text{Qr}}^0 = 0.32 \text{ mM}$

to reveal the stages preceding the nanoparticle formation, the process should be slowed down by reducing the reagent concentration and/or the hydration extent.

Example of such kind for the ratio  $C_{\text{Cu}}:C_{\text{Qr}} = 5.5:1$  and hydration extent 3.7 is shown in Fig. 2.24. In several minutes after the addition of  $\text{Cu}(\text{NH}_3)_4\text{SO}_4$  water solution, changes of Qr spectrum are observed, testifying to the formation of quercetin complex with  $[\text{Cu}(\text{NH}_3)_4]^{2+}$  ions; the band maximum of the complex lies here around 450 nm. Then, intensity of this band begins to fall, with the simultaneous increase of absorption at  $\lambda < 400$  nm, and also the band is revealed with maximum at 310–320 nm. There is isobestic point around 400 nm that indicates to the direct connection between the diminution of complex concentration and the increase of concentration of the component that absorbs at 310–320 nm. At the same time, absorption increases in the region of 540–600 nm where the band of copper nanoparticles is formed under different system parameters (see Fig. 2.23).

Micellar solution of copper nanoparticles has copper-red color; the same color is inherent to the solutions of copper nanoparticles obtained with traditional chemical reducing agents (see, e.g., Chap. 1, Sect. 1.3.2, Fig. 1.9). The band maximum lies at  $550 \pm 5$  nm, i.e., in the absorption region characteristic for these nanoparticles (550–570 nm) [156, 278, 279]. Typical absorption spectrum is shown in Fig. 2.25. Comparison with the spectrum of copper nanoparticles produced by the reduction with hydrazine in reverse micelles at the close hydration extent ( $w = 4$ ) [156] shows that the maximum position is almost the same, but in our case, the nanoparticle band is more distinctly expressed, probably owing to the higher level of conversion of the copper atoms and, consequently, to a lower optical density in the UV region due to the lower concentration of the non-reduced metal ions. Absorption at 800 nm (that characterizes the copper oxide concentration in solution) [156] is negligible in both

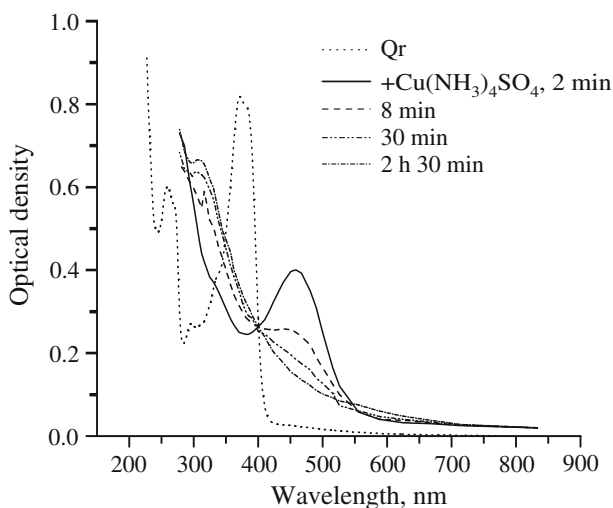
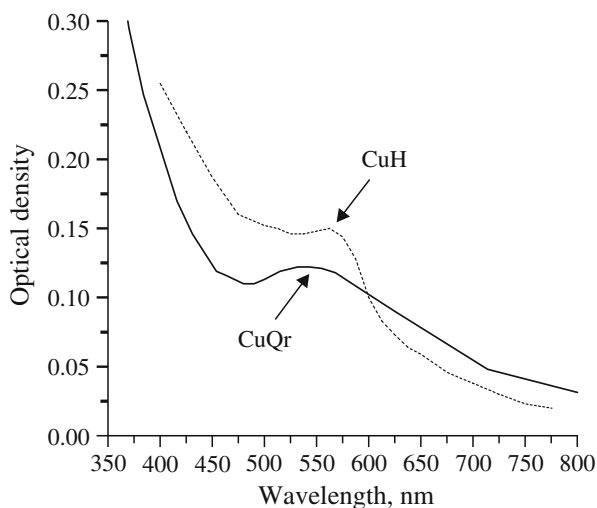


**Fig. 2.24** Cu nanoparticle formation in micellar solution  $C_{\text{Cu}}^0 = 1.64$  mM,  $w = 3.7$ ,  $C_{\text{Qr}}^0 = 0.29$  mM

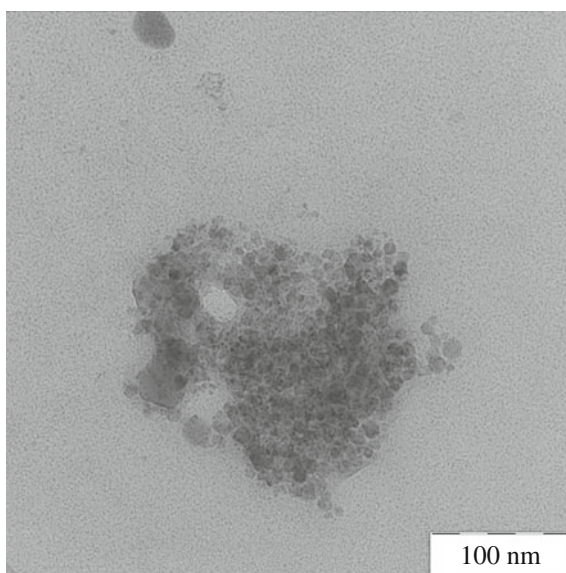
**Fig. 2.25** Absorption spectrum of the copper nanoparticles obtained by biochemical synthesis (CuQr) at the stationary stage,  $w = 3.7$ . For comparison, spectrum is shown of the copper nanoparticles obtained in reverse micelles ( $w = 4$ ) by the reduction with hydrazine (CuH) [156]



cases; this shows that in biochemical synthesis, the nanoparticle oxidation by the atmospheric oxygen is as small as in the synthesis with traditional chemical reducing agent.

It turned out to be extremely difficult to obtain the high-quality TEM images for copper nanoparticles, presumably on account of the small size of the particles and their lower electronic density compared to the previous cases and also probably due to the imperfect procedure used for the sample preparation for microscopy. For today, one of

**Fig. 2.26** Electron micrograph of the Cu nanoparticles in micellar solution. Average particle size does not exceed 15 nm



the most successful attempts is shown in Fig. 2.26. Here, one can see numerous small particles with sizes not exceeding 15 nm, «embedded» in the AOT clot.

The rate of formation and yield of Cu nanoparticles for the same concentrations of reagents and hydration extent are less than those obtained for silver and gold. This is conditioned presumably by the lower degree of quercetin binding with copper ions, detected in studies of metal ion adsorption from aqueous solution by polymer membranes containing quercetin [280].

The PCS analysis of copper nanoparticles in micellar solutions gives a bimodal distribution with large portion of small particles (with the size of several nanometers). Monomodal distribution corresponding to the electron microscopy data could not be obtained in this case, probably due to the low nanoparticle concentration and, accordingly, low intensity of the useful signal.

Copper nanoparticles in micellar solution are stable for at least several months, which allows to use them successfully for the modification of liquid-phase and solid materials (see Chap. 5).

Biological Effects of Metal Nanoparticles

Egorova, E.M.; Kubatiev, A.A.; Schvets, V.I.

2016, XVI, 292 p. 159 illus., 26 illus. in color., Hardcover

ISBN: 978-3-319-30905-7